Adaptive quadtree simulation of sediment transport

Citation for published version:
Soulsby, RL, Borthwick, AGL & Huang, J 2010, 'Adaptive quadtree simulation of sediment transport' Proceedings of the ICE - Engineering and Computational Mechanics, vol 163, no. 2, pp. 101-110. DOI: 10.1680/eacm.2010.163.2.101

Digital Object Identifier (DOI):
10.1680/eacm.2010.163.2.101

Published In:
Proceedings of the ICE - Engineering and Computational Mechanics

Editorial Manager(tm) for Engineering and Computational Mechanics
Manuscript Draft

Manuscript Number: EACM-D-09-00008R1

Title: Adaptive Quadtree Simulation of Bed Morphological Change

Article Type: Paper

Corresponding Author: Professor A G L Borthwick, PhD DSc CEng FICE

Corresponding Author's Institution: University of Oxford

First Author: Jingmin Huang, DPhil

Order of Authors: Jingmin Huang, DPhil; A G L Borthwick, PhD DSc CEng FICE; Richard L Soulsby, MSc

Abstract: Morphodynamic change is a key factor in the development of river systems. This paper describes a two-dimensional model of fluvial bed morphodynamics, with the flow hydrodynamics represented by the hyperbolic nonlinear shallow water equations and the bed morphodynamics by the bed deformation equation. Bed load transport is estimated using a simple expression. Suspended sediment transport is not considered. The model uses a deviatoric form of the nonlinear shallow water equations that mathematically balances the source and flux gradient terms at equilibrium, including the effects of non-uniform bed topography. The governing equations are solved in a decoupled way, using a Godunov-type finite volume solver for the nonlinear shallow water equations and second-order finite differences for the bed deformation equation, both based on adaptive quadtree grids. The evolution of a sandbar in an open channel is tested against generalized approximate analytical solutions. The numerical predictions on adaptive quadtree grids are found to be in excellent agreement with the approximate analytical solutions within the range of validity of the latter. Results are also presented for the evolution of a sand dune and a sand pit. It is demonstrated that the de-coupled shallow flow and bed morphodynamics calculations are computationally efficient and accurate. It is shown that the use of adaptive quadtree grids leads to a much improved computational performance over that on an equivalent fine resolution fixed uniform grid.

Adaptive Quadtree Simulation of Sediment Transport and Morphological Change due to Shallow Flows

Jingmin Huang DPhil [a], Alistair G.L. Borthwick CEng, PhD, DSc, FICE [a*], Richard L. Soulsby MSc [b]

[a] Department of Engineering Science, University of Oxford, Parks Road, Oxford OX1 3PJ, UK

[b] Visiting Professor, Dept of Engineering Science, University of Oxford, Parks Road, Oxford OX1 3PJ, U.K. and Technical Director, HR Wallingford, Howbery Park, Wallingford, OX10 8BA, U.K

ABSTRACT

Morphodynamic change is a key factor in the development of river systems. This paper describes a two-dimensional model of fluvial bed morphodynamics, with the flow hydrodynamics represented by the hyperbolic nonlinear shallow water equations and the bed morphodynamics by the bed deformation equation. Bed load transport is estimated using a simple expression. Suspended sediment transport is not considered. The model uses a deviatoric form of the nonlinear shallow water equations that mathematically balances the source and flux gradient terms at equilibrium, including the effects of non-uniform bed topography. The governing equations are solved in a decoupled way, using a Godunov-type finite volume solver for the nonlinear shallow water equations and second-order finite differences for the bed deformation equation, both based on adaptive quadtree grids. The evolution of a sandbar in an open channel is tested against generalized approximate analytical solutions. The numerical predictions on adaptive quadtree grids are found to be in excellent agreement with the approximate analytical solutions within the range of validity of the latter. Results are also presented for the evolution of a sand dune and a sand pit. It is demonstrated that the de-coupled shallow flow and bed morphodynamics calculations are computationally efficient and accurate. It is shown that the use of adaptive quadtree grids leads to a much improved computational performance over that on an equivalent fine resolution fixed uniform grid.

* Corresponding author. Tel.: +44-1865-273047; Fax: +44-1865-273010.
E-mail address: alistair.borthwick@eng.ox.ac.uk .

Key Words: morphodynamics, shallow water equations; bed load, Godunov-type scheme; approximate Riemann solver; adaptive quadtree grid

NOTATION

A	bed-load sediment transport coefficient
C_{D}	skin friction drag coefficient
Co	Courant number
D	water depth at the inflow boundary
ds	side length of the cell
f	Coriolis parameter
$\mathbf{f}(\mathbf{u})$	flux vector
g	acceleration due to gravity
$\mathbf{g}(\mathbf{u})$	flux vector
H	apex height of dune or bar
h	total water depth
h_{b}	bed elevation
h_s	still water depth
i, j	cell spatial indices
L	dimension of square (quadtree) domain
lev	cell subdivision level
M	cell index at outlet
m	power index
n	time index
q_{bx}, q_{by}	bedload
q_{o}	inflow flux
q_{sx}, q_{sy}	suspended load
q_{tx}, q_{ty}	total volumetric sediment transport rate components
S_{ox}, S_{oy}	bed slope components
$\mathbf{s}(\mathbf{u})$	source term vector
T	morphodynamic time-scale

t time

$\mathbf{u}$ vector of conserved variables

U , V depth-averaged velocity components

U_0 depth-averaged inflow velocity

x, y Cartesian horizontal spatial coordinates

x_0, x_1, x_2 prescribed locations in the x-direction

z_0 bed roughness length

Δt hydrodynamic time step

ΔT morphodynamic time step

Δx, Δy spatial cell sizes in x, y directions

ε bed porosity

η free surface elevation above still water level

τ_{wx} , τ_{wy} stress components at the water surface

τ_{bx} , τ_{by} stress components at the bed

ν eddy viscosity coefficient

ρ fluid density

Δ magnitude of bed level gradient

1. INTRODUCTION

River bed evolution involves complex 3-D interactions between the flow and the bed sediment, including sediment transport, erosion and deposition, and feedback between the changing bed morphology and flow field. A major challenge is to provide accurate predictions of the physical processes while propagating changes in bed level over a broad range of space and time scales. The basic structure of morphodynamic models consists of sub-models for the hydrodynamic and sediment transport processes. The sediment conservation law is generally used to determine changes in bed level (see e.g. Nicholson *et al.*[1]). Proper coupling of the hydrodynamic model and sediment transport model including the sediment conservation law is essential for accurate long-term simulation.

Hudson and Sweby [2] developed a 1-D morphodynamic numerical model to simulate the evolution of a mound, using coupled and decoupled numerical approaches. Hudson and Sweby considered five different Godunov-type formulations, each of which included a flux-limited version of Roe's approximate Riemann solver to remove spurious oscillations at cell interfaces. The numerical predictions were compared with an approximate analytical 1-D bed deformation solution obtained following De Vriend [3]. Hudson and Sweby indicated that of all the formulations, the decoupled steady approach is most accurate. Furthermore, Hudson and Sweby [4] present a detailed overview of explicit Godunov-type numerical methods for solving 1-D morphodynamical systems, and suggest improved Lax-Wendroff and high resolution schemes with equilibrium balancing based on the coupled hydrodynamics and bed deformation equations.

Depth-integrated 2DH models are applicable to flow domains in which there is relatively simple monotonic vertical variation in the velocity, such that a depth-averaged value is representative. Examples include tidal flows in well-mixed estuaries and coastal areas. In a paper on the mathematical modelling of morphological evolution, De Vriend [3] provided useful advice on how to construct a 2DH numerical model. De Vriend pointed out that three major issues needed to be considered: a) the predictive ability of the constituent models when applied to a given situation; b) the balance of the compound models as to physical reliability and numerical accuracy; and c) the appropriate interaction of the constituent models, both physically and numerically. A considerable number of 2DH morphodynamics models have been developed in the past thirty or so years (see Fleming and Hunt [5]; Yamaguchi and Nishioka [6]; O'Connor and Nicholson [7], Wang *et al*. [8], de Vriend [9]; Tanguy and Zhang [10]; Van Wijngaarden [11]; Grunnet *et al*. [12]).

In the present paper, a 2DH morphodynamic numerical model is described based on a deviatoric form of the hyperbolic nonlinear shallow water equations and the bed deformation equation, which mathematically balances the flux and source terms at equilibrium. The equations are discretised on a quadtree grid using a Godunov-type finite volume scheme with either HLL or Roe's approximate Riemann solver (Toro [13]). A first order upwind method is used for simulation of the evolution of a sand bar, a sand dune and hole.

2. GOVERNING EQUATIONS

2.1 Hydrodynamics

The two-dimensional shallow water equations are the depth-averaged version of the Reynolds averaged Navier Stokes equations. They are applicable to nearly horizontal flows with negligible vertical acceleration, such as large-scale flood waves where the wavelength is much larger than the water depth. The two-dimensional nonlinear shallow water equations may be derived by depth-integrating the three-dimensional Reynolds-averaged Navier-Stokes equations, neglecting the vertical acceleration of water particles, and taking the pressure distribution to be hydrostatic. Expressed in matrix form as a system of conservation laws given by Rogers *et al.* [14, 15], a conservation law of the two-dimensional non-linear shallow water equations may be written as

$$\frac{\partial \mathbf{u}}{\partial t} + \frac{\partial \mathbf{f}}{\partial x} + \frac{\partial \mathbf{g}}{\partial y} = \mathbf{s}\,, \tag{1}$$

in which the vector of conserved variables, $\mathbf{u}$, the flux vectors, $\mathbf{f}(\mathbf{u})$ and $\mathbf{g}(\mathbf{u})$, and the source term vector, $\mathbf{s}(\mathbf{u})$, are

$$\mathbf{u} = \begin{bmatrix} \eta \\ Uh \\ Vh \end{bmatrix}, \mathbf{f} = \begin{bmatrix} Uh \\ U^2 h + \frac{1}{2} g(\eta^2 + 2\eta h_s) - \nu h \frac{\partial U}{\partial x} \\ UVh - \nu h \frac{\partial V}{\partial x} \end{bmatrix}, \mathbf{g} = \begin{bmatrix} Vh \\ UVh - \nu h \frac{\partial U}{\partial y} \\ V^2 h + \frac{1}{2} g(\eta^2 + 2\eta h_s) - \nu h \frac{\partial V}{\partial y} \end{bmatrix} \tag{2}$$

$$\text{, and } \mathbf{s} = \begin{bmatrix} 0 \\ (\tau_{wx} - \tau_{bx})/\rho - g\eta S_{ox} + hfV \\ (\tau_{wy} - \tau_{by})/\rho - g\eta S_{oy} - hfU \end{bmatrix}.$$

where η is the free surface elevation above the still water level, U and V are depth-averaged velocity components, h $(= h_s + \eta)$ is the total water depth, h_s is the still water depth, f is the Coriolis parameter related to the Earth's rotation, τ_{wx} and τ_{wy} are the surface stress components, τ_{bx} and τ_{by} are the bed stress components, S_{ox} and S_{oy} are the bed slope components, ν is the eddy viscosity coefficient, g is the acceleration due to gravity, ρ is the

fluid density, t is time, and x and y are horizontal distances in the Cartesian system. The bed stress terms τ_{bx} and τ_{by} represent the energy dissipation influence of bed roughness on the flow and are estimated empirically from

$$\tau_{bx} = \rho C_D U \sqrt{U^2 + V^2}\,, \quad \text{and } \tau_{by} = \rho C_D V \sqrt{U^2 + V^2} \tag{3}$$

When bed deformation is considered, the skin friction drag coefficient $C_{\mathrm{D}} = \left[\dfrac{0.40}{1 + \ln(z_0 / h)}\right]^2$ (Soulsby [16]), in which z_0 is the bed roughness length.

The nonlinear shallow water equations (1) and (2) expressed in matrix hyperbolic conservation form are solved to give updated values for the dependent variables using a standard Godunov-type finite volume scheme. Interface fluxes are evaluated using either HLLC or Roe's approximate Riemann solver (see Toro [13] for a full description of these schemes). The hydrodynamic time step is Δt, and is chosen to satisfy the Courant condition, such that

$$\Delta t \le \min\left(\frac{\mathrm{Co}\,\Delta x}{\sqrt{gh} + U}\right), \ (0 < \mathrm{Co} \le 1 \text{, normally 0.6-0.8 is used}). \tag{4}$$

2.2 Sediment Transport

The sediment transport equations described here apply to non-cohesive sediment at low concentration in liquid of constant density. In two horizontal dimensions, for the equilibrium (or near-equilibrium) condition, the sediment budget equation ignoring "storage" of suspended sediment can be written as (Soulsby [16]),

$$\frac{\partial h_{\mathrm{b}}}{\partial t} = -\frac{1}{1-\varepsilon}\left(\frac{\partial q_{\mathrm{tx}}}{\partial x} + \frac{\partial q_{\mathrm{ty}}}{\partial y}\right), \tag{5}$$

where h_{b} is the bed elevation, ε is the bed porosity, q_{tx}, q_{ty} are components of total volumetric sediment transport rate in the positive x, y directions, and are the sum of suspended load q_{sx}, q_{sy}, and bedload q_{bx}, q_{by}. Only bedload transport is considered in the present problem, and so $q_{\mathrm{tx}} = q_{\mathrm{bx}}$, and $q_{\mathrm{ty}} = q_{\mathrm{by}}$.

The bed deformation equation is discretised spatially at cell i, j using finite differences on a locally uniform grid template, such that

$$\left.\frac{\partial h_{\mathrm{b}}}{\partial t}\right|_{i,j} = -\frac{1}{1-\varepsilon}\left(\left.\frac{\partial q_{\mathrm{tx}}}{\partial x}\right|_{i,j} + \left.\frac{\partial q_{\mathrm{ty}}}{\partial y}\right|_{i,j}\right) \tag{6}$$

Because the central difference method tends to create spurious (and possibly unstable) bed undulations (see e.g. Huang *et al*. [17]), the discretised values of $\frac{\partial q_{\mathrm{tx}}}{\partial x}$ and $\frac{\partial q_{\mathrm{ty}}}{\partial y}$ of cell *i*, *j* are computed by a first order upwind difference method (e.g. Callaghan *et al*. [18]) as

$$\left.\frac{\partial q_{\mathrm{tx}}}{\partial x}\right|_{i,j} = \frac{q_{\mathrm{tx}(i,j)} - q_{\mathrm{tx}(i-1,j)}}{2\Delta x}, \quad \text{if} \quad q_{\mathrm{tx}(i,j)} \geq 0 \tag{7}$$

and

$$\left.\frac{\partial q_{\mathrm{tx}}}{\partial x}\right|_{i,j} = \frac{-q_{\mathrm{tx}(i,j)} + q_{\mathrm{tx}(i+1,j)}}{\Delta x}, \quad \text{if} \quad q_{\mathrm{tx}(i,j)} < 0 \tag{8}$$

where Δx and Δy are cell widths in the *x*- direction, and similar in *y*- direction. A second order Adams-Bashforth time-stepping numerical solver is applied to integrate the discretised bed deformation equation (6) in time. Because the bed level changes slowly compared to the hydrodynamic time step, the bed deformation model is not invoked at every time step of the hydrodynamic model. This is in order to provide sufficient time for the flow velocity to reach a near-equilibrium state and hence to reduce oscillations in the flow field, as well as for computational efficiency. The morphodynamic time step ΔT for the bed deformation model is taken to be between 100 and 500 times the hydrodynamic time step Δt in the cases considered herein. Given that the time is $t = n\Delta T$ where the superscript *n* represents the time index, the updated bed level is given by

$$h_{\mathrm{b}(i,j)}^{n+1} = h_{\mathrm{b}(i,j)}^{n} + \Delta T\left(\frac{3}{2}\left.\frac{\partial h_{\mathrm{b}}}{\partial t}\right|_{i,j}^{n} - \frac{1}{2}\left.\frac{\partial h_{\mathrm{b}}}{\partial t}\right|_{i,j}^{n-1}\right) \tag{9}$$

Predictions of the flow and bed changes are made using a decoupled approach, whereby the nonlinear shallow water equations are solved separately from the bed deformation equation. The hydrodynamic module predicts velocities and water depth at each cell, using centre and face values. The sediment module utilises values of q_{t} at each cell centre. Then the new bed level h_{b} is computed from (9) and (6). The still water datum is constant, and so h_{s} is calculated according to the new bed level from,

$$h_{s(i,j)}^{n+1} = h_{s(i,j)}^{n} + h_{b(i,j)}^{n} - h_{b(i,j)}^{n+1} \tag{10}$$

in which h_s^{n+1} and h_b^{n+1} are the updated still water depth and bed level values at the cell (i, j) centre. Hence, h_s^{n+1} provides feedback to the hydrodynamic model. At first, the combined model switches on solely the hydrodynamic part. Later when the flow is steady, the bed deformation part is also implemented and the bed changes are computed every ΔT.

The following simple transmissive relations are used for inflow and outflow hydrodynamic and morphodynamic boundary conditions (Toro [13]),

$$h_0 = h_1,\ U_0 = U_1,\ h_{b0} = h_{b1} \quad h_M = h_{M\text{-}1},\ U_M = U_{M\text{-}1},\ h_{bM} = h_{bM\text{-}1} \tag{11}$$

In the above, subscripts 0 and 1 refer to the grid points aligned normal to the inflow boundary, such that 0 is immediately outside the boundary, and 1 is immediately inside the flow domain. Subscripts *M* and *M*-1 have similar meaning, and apply at the outlet.

3. DYNAMICALLY ADAPTIVE QUADTREE GRID

The shallow water equations and bed deformation equation are discretised using finite volumes on dynamically adaptive structured quadtree grids. The first step in quadtree grid generation is definition of the computational domain using seeding points based on the initial bathymetry. Next, the cell is successively divided according to seeding point density and boundary identification. If more than one seeding point is located within a cell, the cell is subdivided into four quadrant cells unless the cell is already at the maximum specified subdivision level. The resulting grid is highly resolved in the vicinity of the seeding points, and may have very large differences in cell size and configurations of neighbouring cells. The third step is grid regularisation and minimum division in order to control the local variation in grid density. Starting from the second highest level, each parent cell is examined in turn and subdivided if any of its adjacent and corner neighbour cells is less than half the size. This is undertaken in a single sweep through the quadtree. It helps to reduce the complexity of the local cell layout, thus improving computational efficiency. Furthermore, an extra function (if required) can be implemented to check that there is minimum division in certain areas of interest within the flow domain to provide sufficient computational accuracy.

When the mesh is generated, cell information (e.g. neighbour references, parent and child cell pointers) is automatically stored using a hierarchical data structure, which can be interrogated to locate neighbour cells during grid regularisation and adaptation during the whole simulation. The size of a cell is calculated via

$$ds = \frac{L}{2^{\mathrm{lev}}}, \tag{12}$$

where ds is the side length of the cell, L is the dimension of the square domain, and lev is the subdivision level of the cell. The data structure is updated when implementing dynamic refinement and removal of grid cells according to specified adaptation criteria during the simulation, thus providing a locally high resolution, dynamically adaptive evolving grid. Greaves and Borthwick [19], Liang *et al.* [20], and Huang [21] give a full description of the quadtree grid generation procedure.

4. 2-D BED EVOLUTION TEST RESULTS

4.1 Sandbar

This case is simply the 2-D analogue of Hudson and Sweby's [2] 1-D bed deformation test, which has an approximate analytical solution. We define x, y as distances along the open channel in the stream-wise and transverse directions respectively, with the origin at the inflow boundary. The channel initially has a flat, horizontal bed except for a bar of apex height H located between x_1 and x_2. The initial water depth, and flow velocity conditions are set as,

$$h(x,y)\big|_{t=0} = D - h_{\mathrm{b}}(x,y)\big|_{t=0}, \tag{13}$$

and

$$U(x,y)\big|_{t=0} = \frac{q_{\mathrm{o}}}{h(x,y)\big|_{t=0}}, \tag{14}$$

where q_{o} is a constant inflow flux, D is the water depth at the inflow boundary (thus defining the datum), $h(x, y)$ is the water depth, $U(x, y)$ is the flow velocity, and $h_{\mathrm{b}}(x, y)$ is the bed elevation above the given datum, and t is time. We make the same rigid-lid assumption as

Hudson and Sweby [2] used, which is only valid for U small, $H << D$, and h_b slowly changing. For a given bed elevation, the velocity is determined as,

$$U(x,y)\big|_t \approx \frac{q_o}{D - h_b(x,y)\big|_t} \quad . \tag{15}$$

In this paper, $q_o > 0$, and $U(x,y) > 0$, and the sediment transport is purely by bed load, with the volumetric bed-load sediment transport flux given by (see e.g. Chesher *et al*. [22]),

$$q_b(x,y) = A\left[U(x,y)\big|_t\right]^m \ . \tag{16}$$

The coefficient A has dimensions $m^{2-m}s^{m-1}$; in which m is a power (whose range $3 \le m \le 5$ corresponds to experimental data). Utilising the rigid lid assumption, (16) becomes

$$q_b(x,y)\big|_t \approx A q_o{}^m \left(D - h_b(x,y)\big|_t\right)^{-m}, \tag{17}$$

The 2-D sandbar has the same profile as the 1-D case considered by Hudson and Sweby [2, 4] with initial bed elevation given by

$$h_b(x_0,y_0)\big|_{t=0} = \begin{cases} H\sin^2\left(\dfrac{\pi(x_0 - x_1)}{x_2 - x_1}\right) & \text{if} \quad x_1 \le x_0 \le x_2 \\ 0 & \text{otherwise} \end{cases} \tag{18}$$

The flow domain is of length 1000 × 1000 m, x_1 = 300 m, x_2 = 500 m, D = 10 m, H = 1 m, m = 3, q_o = 10 m^2/s, and ε = 0.4. According to Hudson and Sweby [2, 4] and Huang *et al*. [17], the bed deformation equation can be treated as *a quasi-linear wave equation*, and so the movement of the sand bar is given by:

$$h_b(x,y)\big|_t = h_b(x_0,y_0)\big|_{t=0} \tag{19}$$

with
$$x = x_0 + \frac{t}{T} D \begin{cases} \left[1 - \dfrac{H}{D}\sin^2\left(\dfrac{\pi(x_0 - x_1)}{(x_2 - x_1)}\right)\right]^{-(m+1)} & \text{if} \quad x_1 \le x_0 \le x_2 \\ 1 & \text{otherwise} \end{cases} \tag{20}$$

and T is defined as the morphodynamic time-scale (Huang *et al*. [17]),

$$T = \frac{(1-\varepsilon)\, D^{m+2}}{A\, m\, q_o{}^m} = \frac{(1-\varepsilon)\, D^2}{A\, m\, U_o{}^m} \ . \tag{21}$$

where $U_0 = q_0/D$. The approximate solution of the bed deformation h_b is valid until t/T reaches a maximum value of $t/T \le 11.9$. Hudson and Sweby expressed this in terms of A as $t \le 238/A$.

A comparison is made between the numerical model predictions of morphodynamic change and the corresponding approximate analytical solutions using dynamically adaptive quadtree grids and uniform grids. The hydrodynamics are computed using the Godunov-type finite volume scheme with an HLLC approximate Riemann solver. The hydrodynamic time step is $\Delta t = 0.1$ s. The bed deformation equation is solved using upwind differences. In this case, the coefficient $A = 0.01$ s^2/m. The bed level update time step $\Delta T = 50\Delta t$ in this case. In order to be consistent with the analytical model, bed friction, surface, and (viscous) effective stresses are not included. The Coriolis force is also neglected. The numerical simulation is first run for an initial 1000 s with the bed and mesh fixed in order to reach a steady hydrodynamic state, at which point the time is set to t = 0 s. The bed deformation model is then switched on.

The initial quadtree grid is divided between 5 and 8 levels ($\Delta x = 31.25$ and 3.91 m respectively). Figure 1 (a) shows the initial quadtree grid. The quadtree grid is dynamically adapted according to the magnitude of the bed level gradient,

$$\Delta = \sqrt{\left(\frac{\partial\, h_b}{\partial x}\right)^2 + \left(\frac{\partial\, h_b}{\partial y}\right)^2}\ . \tag{22}$$

If Δ exceeds or is equal to 0.0003, a cell is divided into four. If all four cells sharing the same parent satisfy Δ < 0.0001, the four cells are removed. The maximum division level is 8 and minimum level is 5. Linear interpolation is used to create a local discretisation template with the same level for each cell. Renewal of the mesh is only implemented whenever the bed level is calculated and updated, and only one level more or less allowed for coarsening or refining. Figure 1(b) shows the adapted quadtree grid at t = 238/A.

The 2-D sandbar case was run on a fixed uniform grid of 8-level division until t = 238/A using the first-order upwind difference scheme. Figure 2 shows the bed level profiles obtained by the approximate analytical solution, fixed grid and adaptive grid. The prediction obtained on the adapted quadtree grid is very close to that from the fixed grids using the highest level. Use of the adapted quadtree grid improves the computational time by 60%

while retaining accuracy. It should be noted that the predictions by the first order upwind method introduce artificial diffusion, causing the noticeable reduction in amplitude of the sand wave. In practice, this could be improved by using second order upwind method.

4.2 Sand-Dune

The second 2-D case involves the evolution of a sediment bank resembling a dune on an otherwise horizontal erodible bed (Hudson and Sweby [4]). For this problem no approximate analytical solution is available. The overall plan dimensions of the domain are 1500 m longitudinal by 1000 m transverse, with respect to the channel. All other initial conditions are set the same as the 1-D case. The numerical model is first run to hydrodynamic steady state for a fixed bed from the following initial water depth, flow velocity and bed profile conditions:

$$h_{\mathrm{b}}(x,y)\big|_{t=0} = \begin{cases} \sin^2\left(\dfrac{\pi(x-500)}{200}\right)\sin^2\left(\dfrac{\pi(y-400)}{200}\right) & \text{if } 500 \le x \le 700,\ 400 \le y \le 600 \\ 0 & \text{otherwise} \end{cases} \qquad (23)$$

Figure 3 (a) shows the initial bed level contours and 3-D view of the bed surface.

The simulation is undertaken on a uniform grid with a maximum of 8-level division. The coefficient A is set equal to 0.01 s^2/m, m = 3, with morphodynamic time-scale T = 2000s. The simulation run time is until t = 20 hours. This case should be exactly equivalent to a simulation period of t = 200 hours with A = 0.001 s^2/m (T = 20000s) used by Hudson and Sweby [4]). Figure 3(b) shows the bed level contours and 3-D view at t = 20 hours.

Convergence of the numerical solution is examined for grid division levels 4, 5, 6, and 7 against level 8. Figure 4 illustrates the bed level contours obtained on the different grids. It is obvious that the level 4 and 5 grids give too coarse a representation of the evolved bedform. The results on the level 6 and 7 grids indicate that the plan shape has the lateral wings usually associated with the migrating dune. The contour plot for the level 8 grid includes the rear indent in agreement with Hudson and Sweby [4].

The 2-D sand dune case has been modelled on a dynamically adaptive quadtree grid where cell refinement is according to bed gradient (expressed by Eq. (22) with the same criteria for the enrichment and coarsening). The maximum division is 8- and the minimum is 5- level. Figure 5 shows the adapted quadtree grids, bed level contours and 3-D views at t = 1h and 2h. The dune evolves to have an arrow-head or chevron like shape in plan, with a steep upstream front, shallower sloped tail and sideways protrusions. The result is very similar to the prediction obtained on the reference uniform grid.

The CPU time for the simulation on the adapted grid using the first-order upwind method and 5 to 8 level division is around 20% of the time and 30% of storage required by an 8-level uniform grid. Use of the adapted quadtree grid therefore speeds up the computational process while retaining accuracy. Obviously the smaller the cell dimension the better the accuracy of the predictions in the range of grid convergence (Huang *et al*. [17]). This advantage becomes more significant when the computational domain is large and the simulation time is long. Figure 6 shows the error (expressed as deviation from the solution on the level 8 uniform grid) against relative CPU time for the sand dune case at t = 20 h (A = 0.01 s^2/m) for level 4, 5, 6, and 7 uniform grids and the adaptive quadtree grid. (The CPU time is relative to that on the reference level 8 uniform grid). By inspecting Figure 6, it can be seen that there is a substantial gain in accuracy at a given CPU time if one uses a dynamically adaptive quadtree grid instead of the corresponding resolution uniform grid. The improved computational efficiency means that the present quadtree approach is useful at fast simulation of bed morphodynamics. Moreover, by coarsening the grid in areas of little interest, the local constraint of the Courant condition on the time step is of course reduced.

By comparing Figure 5 to Figure 3, it can be seen that the adaptive quadtree scheme provides a smoother prediction in the region beyond the dune (i.e. no depression in the bed in the lee of the crest of the dune). Numerical stability is improved and uncontrolled dispersion is avoided by using the dynamically adapted quadtree grid.

Hudson and Sweby [4] investigated the sand dune evolution case by considering two approaches, a decoupled approach similar to that used here and a coupled approach with

$\Delta x = \Delta y = 20$ m. Hudson and Sweby declared that in 2D the decoupled approach seemed to provide an inaccurate prediction due to the presence of kinks and the difference in position and shape of the pulse. In the present paper, 8 level divisions are utilised with $\Delta x = 5.86$ m, $\Delta y = 3.91$ m; however, an accurate prediction is obtained using the decoupled approach herein. This example confirms the need for grid resolution.

4.3 Sand Pit

The evolution of a sand pit with an horizontal erodible bed is considered as the third case. The initial bed profile is the mirror image of the dune profile. Again no approximate analytical solution is available. The domain is 1500 × 1000 m. The numerical model is first run to hydrodynamic steady state for a fixed bed using the same initial flow conditions as in the previous test. However, the bed profile is:

$$h_{\mathrm{b}}(x,y)\big|_{t=0} = \begin{cases} -\sin^2\left(\dfrac{\pi(x-500)}{200}\right)\sin^2\left(\dfrac{\pi(y-400)}{200}\right) & \text{if } 500 \le x \le 700,\ 400 \le y \le 600 \\ 0 & \text{otherwise} \end{cases} \tag{24}$$

The simulation is undertaken on an adaptive quadtree grid with the same criteria as the sand dune evolution. The simulation run time is until t = 20 hours. Figure 7 shows the adapted quadtree grid, bed level contours and 3-D view at t = 10 h and 20 h; it can be seen that the pit evolves to have a very similar (but mirrored) shape to that of the sand dune. The bed centreline profiles given in Figure 8 indicate that the dune crest migrates at a slightly faster rate than the trough of the pit. This is to be expected because of feedback between the overlying flow speed and the local depth through continuity. It should be noted that there is no account taken in the present bed load equation of the gravitational effects of bed slope. Inclusion of this effect would lead to additional differences between the dune and pit cases.

5. CONCLUSIONS

This paper has introduced a decoupled 2-D sediment transport model based on a Godunov-type finite volume solver of the shallow water equations and a finite difference solver of the bed deformation equation, with empirical formulae used to estimate the sediment bed load. Validation was undertaken by comparison against an approximate analytical solution for a

benchmark case of the evolution of a sand bar, and reasonable agreement achieved, although the simulated crest was lower than the analytical solution due to the diffusivity of the first order upwind scheme. Further simulations have been presented of the morphodynamic evolution of a sand dune and a sand pit; it is found that the trough of the sand pit migrates at a slightly lower speed than the crest of a corresponding sand wave. The use of dynamically adapted quadtree grids has led to a significant improvement in computational time while retaining accuracy (by comparison with simulations undertaken on a fixed uniform grid of corresponding resolution). As would be expected, use of finer resolution (i.e. higher level) adaptive quadtree grids has enhanced the accuracy and detail of the solutions. The present approach is particularly well suited to applications involving long simulations in large shallow domains. It is recommended that future work be undertaken to enhance the numerical solver to include a higher-order upwind scheme (which will involve further cells in the discretisation template).

ACKNOWLEDGEMENTS

The authors gratefully acknowledge the support provided by the U.K. Engineering and Physical Sciences Research Council through EPSRC Grant GR/S73402, and jointly managed by Dr P H Taylor (Oxford University) and Professor P K Stansby (Manchester University). Dr J G Zhou (Liverpool University) and Professor S Wieprecht (Stuttgart University) gave useful advice that informed the work presented here. The authors are indebted to Jane Palmer and Horace Palmer of IBEX Geotech Ltd, the Oxford Hong Kong Scholarship Fund, the Henry Lester Trust and St Hugh's College Oxford for their support.

REFERENCES

1. NICHOLSON J., BROKER I., ROELVINK J.A., PRICE D., TANGUY J.M. and MORENO L. Intercomparison of coastal area morphodynamic models. *Coastal Engineering*, 1997, **31**, No. 1-4, pp. 97-123.
2. HUDSON J. and SWEBY P.K. Formulations for numerically approximating hyperbolic systems governing sediment transport. *Journal of Scientific Computing*, 2003, **19**, No. 1-3, pp. 225-252.

3. DE VRIEND H.J. 2DH mathematical modelling of morphological evolutions in shallow water. *Coastal Engineering*, 1987, **11**, No. 1, pp. 1-27.
4. HUDSON J. and SWEBY P. K. A high-resolution scheme for the equations governing 2D bed-load sediment transport, *International Journal for Numerical Methods in Fluids*, 2005, **47**, No. 10-11, pp. 1085-1091.
5. FLEMING C.A and HUNT J.N. Application of sediment transport model. In *Proceedings of 15th International Coastal Engineering Conference, Honolulu*, American Society of Civil Engineers, New York, 1976, pp. 1184-1202.
6. YAMAGUCHI M. and NISHIOKA Y. Numerical simulation on the change of bottom topography by the presence of coastal structures. In *Proceedings of 19th International Coastal Engineering Conference*, *Houston*, American Society of Civil Engineers, New York, 1984, Vol. 2, pp. 1732-1748.
7. O'CONNOR B.A. and NICHOLSON J. Modelling changes in coastal morphology. In *Proceedings of International Symposium on Sediment Transport Modeling, New Orleans* (WANG S.S.Y. (editor)), American Society of Civil Engineers, 1989, pp. 160-165.
8. WANG H., MIAO G. and LIN L.H. A time-dependent nearshore morphological response model. In *Proceedings of 23rd International Coastal Engineering Conference*, *Venice*, American Society of Civil Engineers, 1992, pp. 2513-2527.
9. DE VRIEND H.J. Mathematical modelling of coastal morphodynamics. In: *Advanced Series on Ocean Engineering*. World Scientific, Singapore, 1996.
10. TANGUY J.M. and ZHANG B.N. Morphological modeling of the evolution of a trench connecting a lagoon to the sea at Keta, Ghana, In *Proceedings of International Symposium on Waves – Physical and Numerical Modelling*, *Vancouver* (ISAACSON M. and QUICK M. (editors)), IAHR Delft, 1994, pp. 1453-1462.
11. VAN WIJNGAARDEN M. A two-dimensional model for suspended sediment transport in the southern branch of the Rhine-Meuse estuary, The Netherlands. *Earth Surface Processes and Landforms*, 1999, **24**, No. 13, 1173 – 1188.
12. GRUNNET N.M., WALSTRA D.R. and RUESSINK B.G. Process-based modelling of a shore-face nourishment. *Coastal Engineering*, 2004, **51**, No. 7, pp. 581-607.

13. TORO E.F. *Shock-Capturing Methods for Free-Surface Shallow Flows*, John Wiley and Sons Ltd, Chichester, 2001.

14. ROGERS B.D., FUJIHARA M. and BORTHWICK A.G.L. Adaptive Q-tree Godunov-type scheme for shallow water equations, *International Journal for Numerical Methods in Fluids*, 2001, **35**, pp. 247-280.

15. ROGERS B.D., BORTHWICK A.G.L. and TAYLOR P.H. Mathematical balancing of flux gradient and source terms prior to using Roe's approximate Riemann solver, *Journal of Computational Physics*, 2003, **192**, No. 2, pp. 422-451.

16. SOULSBY R.L. *Dynamics of Marine Sands*, Thomas Telford Publications, London, 1997.

17. HUANG J., BORTHWICK A.G.L and SOULSBY R.L. One-dimensional modelling of fluvial bed morphodynamics. *Journal of Hydraulic Research*, 2008, **46**, No. 5, pp. 636-647.

18. CALLAGHAN D.P., SAINT-CAST F., NIELSEN P., BALDOCK T.E. Numerical solutions of the sediment conservation law; a review and improved formulation for coastal morphological modelling. *Coastal Engineering*, 2006, **53**, No. 7, pp. 557-571.

19. GREAVES D.M. and BORTHWICK A.G.L. Hierarchical tree-based finite element mesh generation. *International Journal for Numerical Methods in Engineering*, 1999, **45**, No. 4, pp. 447-471.

20. LIANG Q., BORTHWICK A.G.L. and STELLING G. Simulation of dam- and dyke-break hydrodynamics on dynamically adaptive quadtree grids. *International Journal for Numerical Methods in Fluids*, 2004, **46**, No. 2, pp. 127-162.

21. HUANG J. *Simulation of Shallow Fluvial Morphodynamics*. D.Phil. Thesis, University of Oxford, U.K., 2005.

22. CHESHER T.J., WALLACE H.M., MEADOWCROFT I.C. and SOUTHGATE H.N. *PISCES, A Morphodynamic Coastal Area Model, First Annual Report*. Ref: SR337, HR Wallingford Ltd, 1993.

.

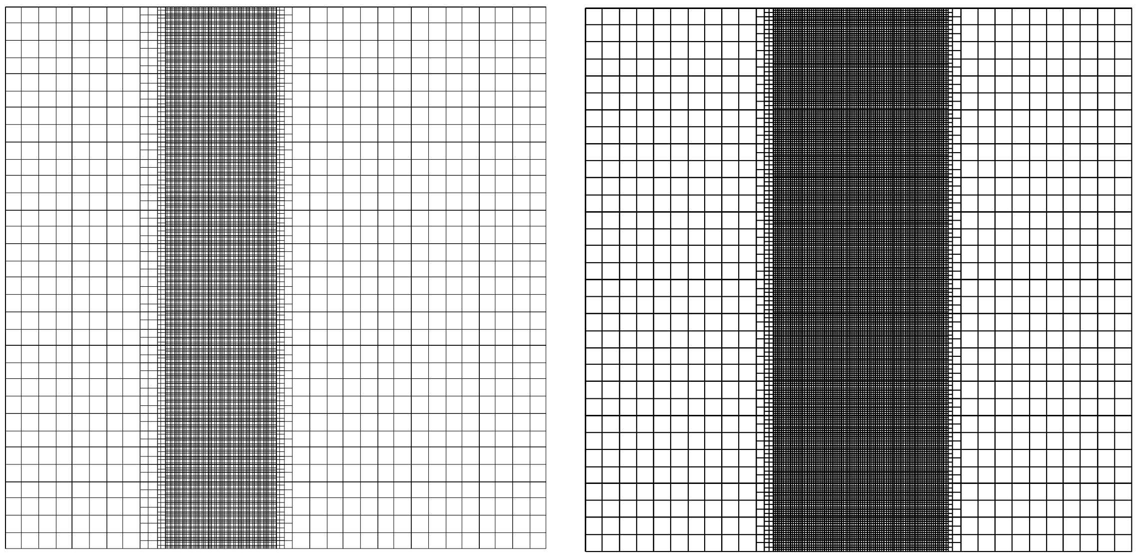

(a) (b)

Figure 1 2-D quadtree grids of sand bar initial state and at t = 238/A (A = 0.01)

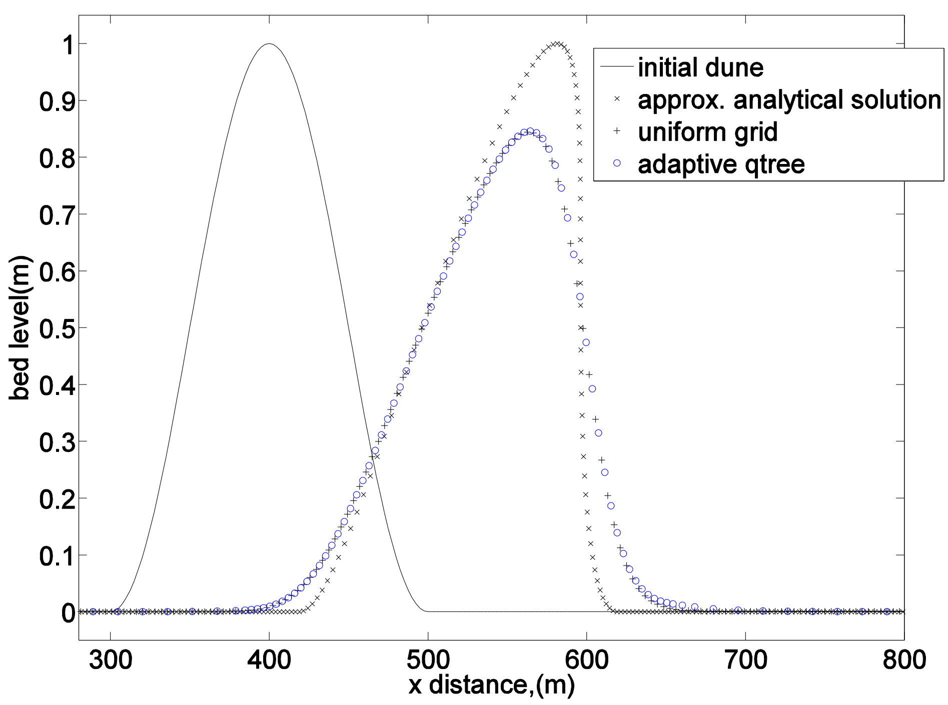

Figure 2 2-D sand bar evolution case: bed level profiles at t = 238/A (A = 0.01)

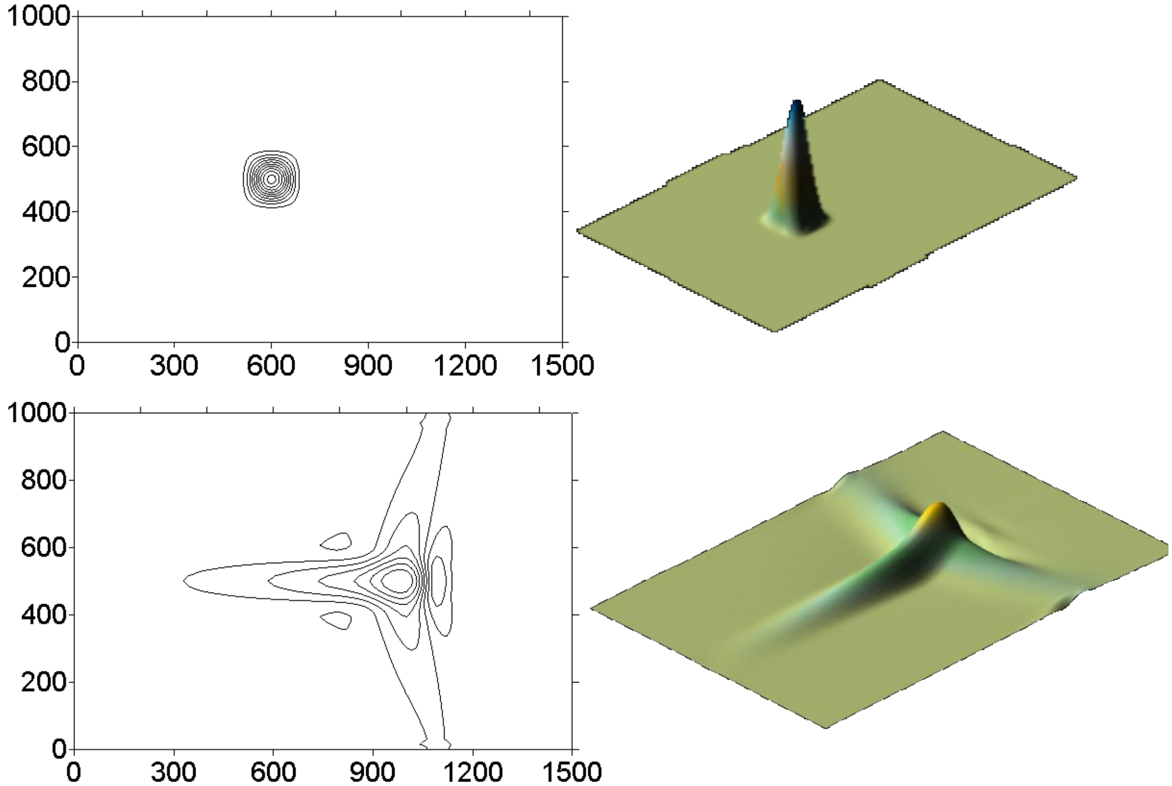

Figure 3   2-D sand dune case: contour and 3d view of initial bed state and bed evolution using upwind method at t = 20 h (A = 0.01)

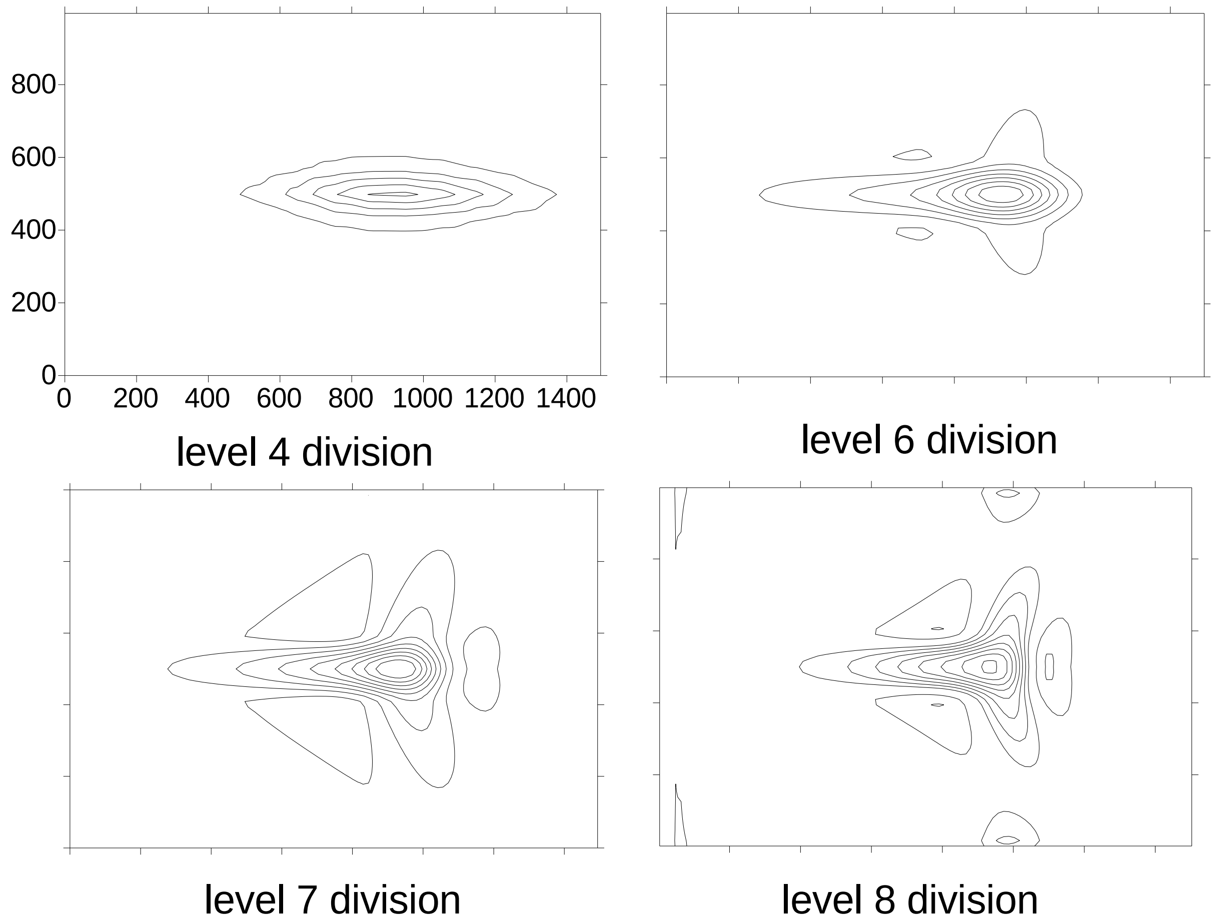

Figure 4   2-D sand dune case: evolved bed contours at t = 20 h (A = 0.01) for different uniform grid division levels

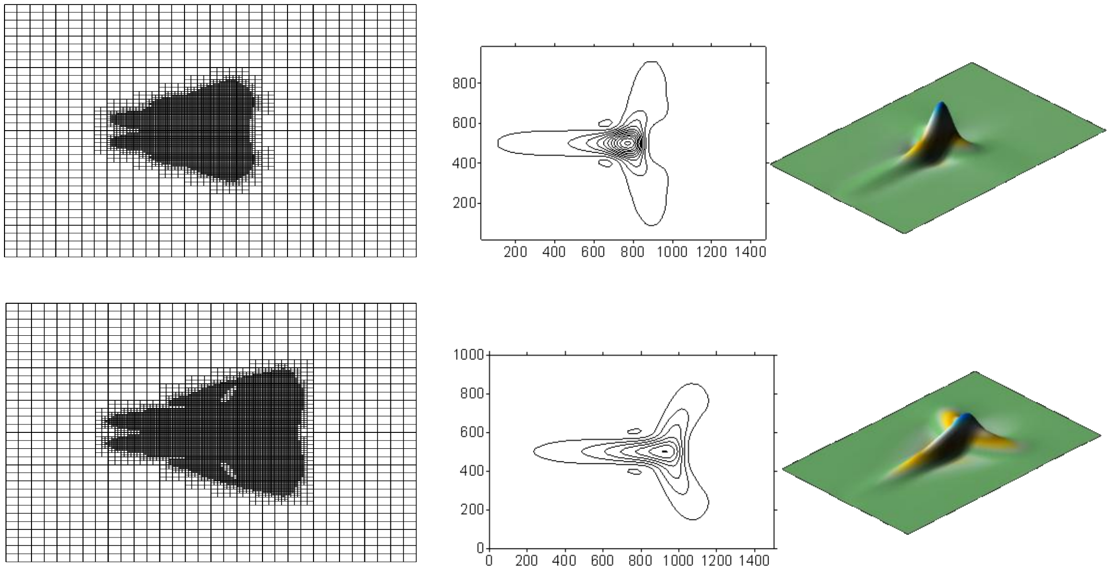

Figure 5 2-D sand dune case: adapted quadtree grids, bed level contour and 3-D view at t = 10 h and t = 20h (5 to 8 grid levels)

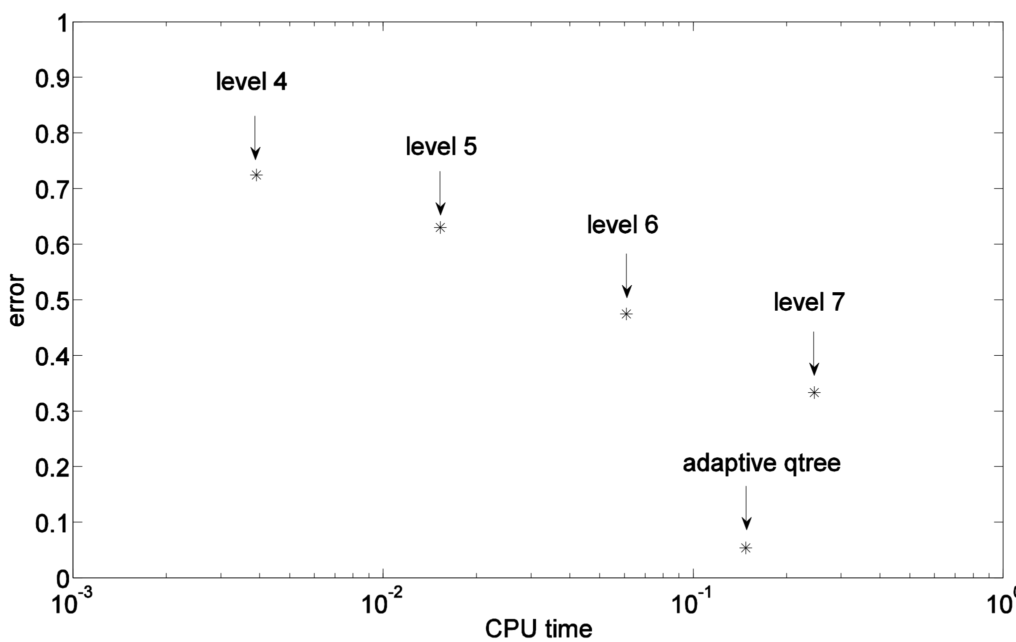

Figure 6 Error and CPU time for 2-D sand dune case at t = 20 h (A = 0.01) for uniform grids at level 4, 5, 6, 7 and adaptive quadtree relative to a uniform grid at level 8

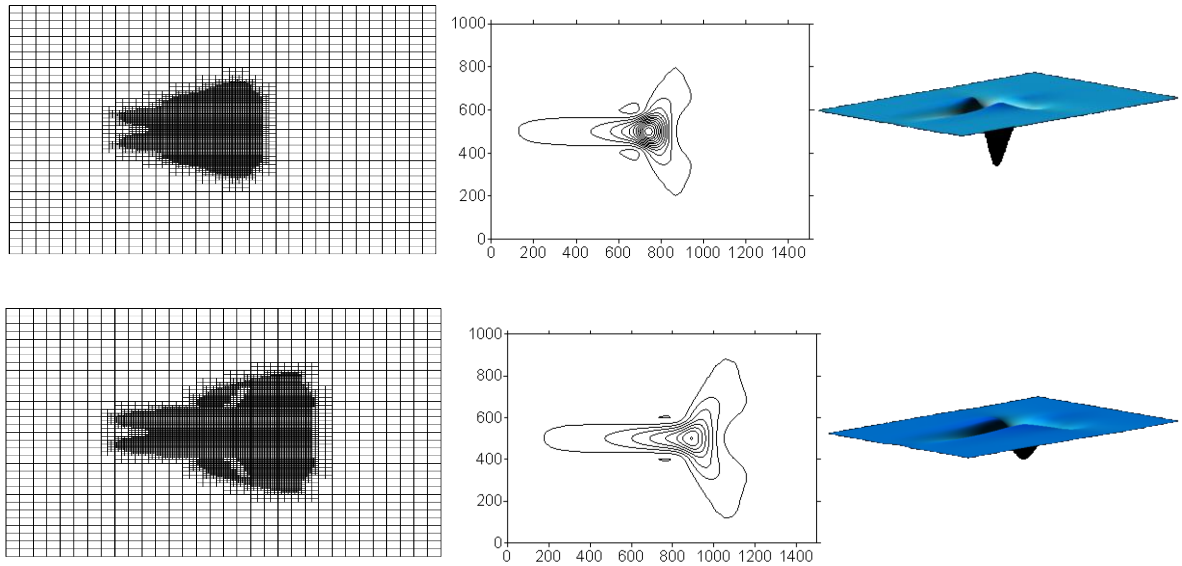

Figure 7 2-D sand hole case: adapted quadtree grids, bed level contour and 3-D view at t = 10h and t = 20h (5 to 8 grid levels)

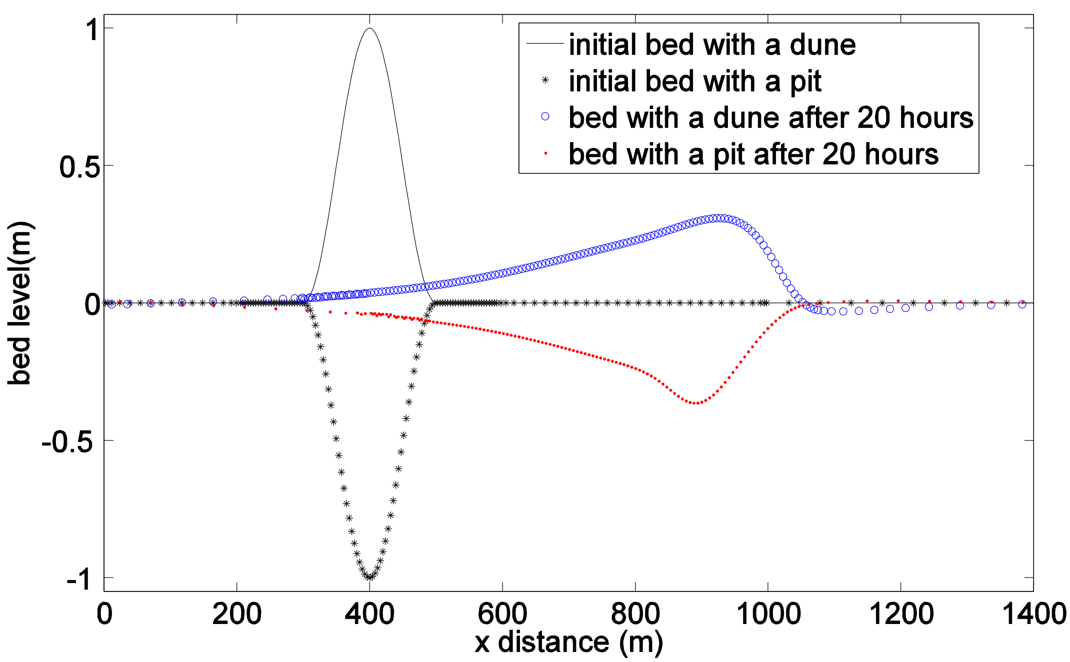

Figure 8 Sand dune and sand hole evolution case: bed level profiles at t = 20h